Structure of open-flavor four-quark states in the charm and bottom region

Joshua Hoffer,[1,2,*] Gernot Eichmann,[3,†] and Christian S. Fischer[1,2,‡]

[1]*Institut für Theoretische Physik, Justus-Liebig-Universität Gießen, 35392 Gießen, Germany*
[2]*Helmholtz Forschungsakademie Hessen für FAIR (HFHF), GSI Helmholtzzentrum für Schwerionenforschung, Campus Gießen, 35392 Gießen, Germany*
[3]*Institute of Physics, University of Graz, NAWI Graz, Universitätsplatz 5, 8010 Graz, Austria*

(Received 20 September 2024; accepted 2 March 2025; published 24 March 2025)

We present quantitative results for masses and the internal structure of four-quark states with two heavy quarks, i.e., $QQ'\bar{q}\bar{q}'$ with $Q, Q' \in \{c, b\}$ and $q, q' \in \{u, d, s\}$, and $J^P \in 1^+$. The composition of these states in terms of meson-meson and diquark-antidiquark pairs, extracted from a relativistic four-body Faddeev-Yakubowski equation, is dynamically determined from underlying QCD forces. We find states at energy levels in very good agreement with lattice QCD and, where available, with experimental states. Their internal structure, most notably between the T_{cc}^+, T_{bc} and $T_{\bar{b}\bar{b}}^-$, show significant and sizeable variations.

DOI: 10.1103/PhysRevD.111.054028

I. INTRODUCTION

It took almost 40 years from the introduction of the notion of "exotic" four-quark mesons [1] until the first such candidate, the $\chi_{c1}(3872)$, was identified by the BELLE Collaboration [2]. Since then, many more exotic meson candidates were discovered by Belle (II), *BABAR*, BES III and the LHCb experiments in the strange, charm and bottom energy region. While some four-quark states have similar quantum numbers and even masses as conventional mesons, many have unique signatures such as carrying an electric charge or conventionally forbidden decay patterns, see Refs. [3–10] for recent review articles.

At the time of writing, all observed hidden-flavor four-quark states with quark content $Q, Q' \in \{c, b\}$ and $q, q' \in \{u, d, s\}$ are resonances that decay predominantly via the strong interaction. The decay widths vary widely from a few to a few hundred MeV [11]. By contrast, open-flavor four-quark states with two heavy quarks and two light antiquarks,[1] i.e., $QQ'\bar{q}\bar{q}'$, are expected to form stable bound states for isospin $I = 0$, provided the mass of the heavy quark pair is sufficiently large and the mass of the light antiquarks sufficiently small [12–16]. The heavy QQ' pair then behaves almost like a pointlike, color-antitriplet antiquark and the resulting binding mechanism is similar as in heavy-light baryons. Indeed, theoretical calculations in recent years find a deeply bound $bb\bar{u}\bar{d}$ four-quark state, called $T_{\bar{b}\bar{b}}^-$, with a binding energy around $-(100\text{–}200)$ MeV with respect to the BB^* threshold, see, e.g., [17–21] and references therein. Its charm-quark counterpart T_{cc}^+ with $cc\bar{u}\bar{d}$ is the only open-flavor state that has been identified experimentally [22,23]. With a binding energy of $-273(61)$ keV with respect to the D^0D^{*+} threshold, this state is extremely shallow and has a narrow decay width of only 410(165) keV.

The internal structure of open-flavor four-quark states is highly debated in the literature. Provided two-body forces are dominant, there are two distinct possibilities: the four (anti)quarks may form heavy-light meson-meson pairs or may arrange in (heavy-heavy)(light-light) diquark-antidiquark pairs. These correlations in flavor and color space may then result in a spatial structure such as meson molecules [7] or compact heavy diquarks [18,19]. For the latter case it has been argued that the formation of a corresponding light scalar diquark-antidiquark pair is an important binding mechanism for the four-quark state.

In order to settle these questions, it is crucial to develop approaches without *a priori* assumptions on the internal structure of these states. This is the main topic of this work. We report on results from functional methods, i.e., from the four-body Faddeev-Yakubowski equation and underlying Dyson-Schwinger equations. In a series of works [24–26] we have shown that the framework is capable of describing the resonant nature of the $f_0(500)$, together with its partners in the lightest scalar meson nonet, and qualitative properties of hidden-flavor heavy-light four-quark states [27–30]. Two-body clusters in the four-body states are

*Contact author: joshua.hoffer@theo.physik.uni-giessen.de
†Contact author: gernot.eichmann@uni-graz.at
‡Contact author: christian.fischer@theo.physik.uni-giessen.de

[1]In this work we consider the strong interaction only. Consequently $QQ'\bar{q}\bar{q}'$ and $\bar{Q}\bar{Q}'qq'$ are equivalent.

dynamically generated by the underlying QCD interactions without prejudice or assumptions on dominant meson-meson or diquark-antidiquark structures. As we will see in the course of this work, this is particularly important as the interplay of flavor structure and resulting symmetries generates different dominant structures for different states. A further crucial, and novel, element compared to previous works in the functional approach is the inclusion of both *attractive and repulsive* meson-meson and diquark-antidiquark configurations. As it turns out, this is mandatory to render our calculation quantitative for states with both $I(J^P) = 0(1^+)$ and $I(J^P) = 1(1^+)$. We furthermore develop the techniques to quantify the contributions of these configurations to the total norm of these states, thus offering important insights into their internal structure.

We briefly summarize our framework in the next section and discuss results for the spectrum and internal structure in Sec. III, before we conclude in Sec. IV. Further technical details are given in the Appendix.

II. FOUR-QUARK EQUATION

The four-body Faddeev-Yakubowski equation is an exact homogeneous Bethe-Salpeter equation (BSE) in QCD. Its solution provides the location of the mass pole in the complex energy plane, i.e., a real mass on the first Riemann sheet for a bound state below threshold or a complex (real) mass on higher sheets for resonances (virtual states). In compact notation it has the generic form

$$\Gamma^{(4)} = K^{(4)} G_0^{(4)} \Gamma^{(4)}, \tag{1}$$

where each multiplication corresponds to an integration over all loop momenta. The interaction kernel $K^{(4)}$ contains all possible two-, three- and four-body interactions, $\Gamma^{(4)}$ is the four-quark Bethe-Salpeter amplitude (BSA), and $G_0^{(4)}$ is the product of four dressed (anti)quark propagators; see [24,27,30,31] for details. Equation (1) is an eigenvalue equation, where the pole locations are identified by the eigenvalue $\lambda_i(P^2)$ of $K^{(4)} G_0^{(4)}$ satisfying $\lambda_i(P^2) = 1$. Here $i = 0$ stands for the ground state and $i = 1, 2, \ldots$ for radially excited states.

The main focus of this work is to study the properties of open-flavor four-quark states in terms of their composition in internal two-body clusters. As in our previous works, we therefore assume dominance of two-body correlations and neglect irreducible three- and four-body interactions [27–29,31]. The interaction kernel then reads

$$K^{(4)} G_0^{(4)} = \sum_{aa'} (K_a + K'_a - K_{aa'}), \tag{2}$$

with a and a' denoting interactions between quark-(anti) quark pairs. The last term in Eq. (2) is necessary to avoid overcounting [24,32,33]. For our case of an open-flavor four-quark state $QQ'\bar{q}\bar{q}'$, with $Q, Q' \in \{b, c\}$ and q, $q' \in \{u, d, s, c\}$, the resulting equation is shown diagrammatically in Fig. 1. The pair aa' can be one of three combinations (12)(34), (13)(24) and (14)(23) corresponding to the possible two-body interaction topologies: One (heavy-heavy)(light-light) diquark-antidiquark $(QQ')(\bar{q}\bar{q}')$ and two heavy-light meson-meson topologies $(Q\bar{q})(Q'\bar{q}')$ and $(Q\bar{q}')(Q'\bar{q})$. For the two-body interaction we employ the rainbow-ladder truncation, where the quark-(anti-) quark kernel is absorbed into an effective gluon exchange. This is the leading order in a systematic truncation scheme and has been successfully used to determine spectra of mesons, baryons and four-quark states in the past, see [34,35] for reviews. The explicit form of the interaction is discussed in Appendix B.

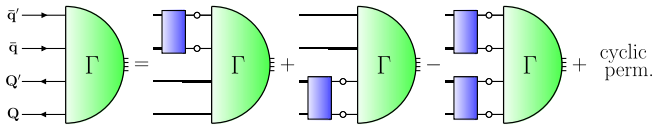

FIG. 1. Four-quark BSE for an open-flavor $QQ'\bar{q}\bar{q}'$ system in the (12)(34) topology; the permutations (13)(24) and (14)(23) are not shown. The green half-circles represent the Bethe-Salpeter amplitudes, blue boxes the two-body interaction kernels and the circles fully dressed quark propagators.

For given quantum numbers J^P, the four-quark Bethe-Salpeter amplitude can be written as

$$\Gamma^{(\mu)}(P, p, k, q) = \Gamma_{\mathrm{D}}^{(\mu)}(P, p, k, q) \otimes \Gamma_{\mathrm{C}} \otimes \Gamma_{\mathrm{F}}, \tag{3}$$

with the total momentum P of the four-quark state and relative momenta p, k, q between the four (anti)quarks. Γ_{D}, Γ_{C} and Γ_{F} are the Dirac, color and flavor parts, respectively. The Lorentz index μ applies to $J = 1$ states.

Following the arguments in [30], we reduce the full BSA, initially containing 256 Dirac structures for $J = 0$ and 768 for $J = 1$, to the physical BSA expressed in terms of the six dominant internal two-body clusters for the different interaction topologies given in Table I:

$$\Gamma^{(\mu)}(S_0, a, s) \approx \sum_{j=0}^{5} f_j(S_0) \tau_j^{(\mu)}(S_0, a, s) \otimes \tau_j^{\mathrm{C}} \otimes \tau_j^{\mathrm{F}}. \tag{4}$$

The dressing functions f_j depend on the permutation-group invariant momentum scale $S_0 = (p^2 + q^2 + k^2)/4$. The Dirac-Lorentz tensors $\tau_j^{(\mu)}$ already include the internal two-body pole structures for the physical components given in Table I and therefore depend on S_0 but also on the doublet variables $a = \sqrt{3}(q^2 - p^2)/4$ and $s = (p^2 + q^2 - 2k^2)/4$. The τ_j^{F} are the flavor tensors for details on momentum dependencies see [28,31]. The τ_j^{C} are the color singlet structures for each interaction topology, where we include the attractive $\mathbf{1} \otimes \mathbf{1}$ and repulsive $\mathbf{8} \otimes \mathbf{8}$ color

TABLE I. Physical content of the BS amplitude for quark and color configurations investigated in this work, with $n \in \{u, d\}$. States with $\bar{c}\,\bar{c}$ are analogous to those with $\bar{s}\,\bar{s}$ and not shown explicitly. Scalar and axial-vector diquarks are denoted by S and A respectively, with the subscript denoting the heavy-quark content of the diquark. We grouped the physical components according to their attractive and repulsive color structure; f_0, f_1, f_2, f_3, f_4, f_5 correspond to the dressing functions for that particular component and color channel. Empty slots in meson-meson channels are not populated for physics reasons, while those in diquark channels are forbidden by symmetry constraints.

		Physical components					
		$\mathbf{1}\otimes\mathbf{1}$		$\bar{\mathbf{3}}\otimes\mathbf{3}$	$\mathbf{8}\otimes\mathbf{8}$		$\mathbf{6}\otimes\bar{\mathbf{6}}$
$I(J^P)$		f_0	f_1	f_2	f_3	f_4	f_5
$0(1^+)$	$bb\bar{n}\bar{n}$	BB^*	B^*B^*	$A_{bb}S$	BB^*	B^*B^*	$S_{bb}A$
	$bc\bar{n}\bar{n}$	BD^*	B^*D	$A_{bc}S$	BD^*	B^*D	$S_{bc}A$
	$cc\bar{n}\bar{n}$	DD^*	D^*D^*	$A_{cc}S$	DD^*	D^*D^*	$S_{cc}A$
	$bb\bar{s}\bar{s}$	$B_sB_s^*$	$\cdots$	$A_{bb}A_{ss}$	$B_sB_s^*$	$\cdots$	$\cdots$
	$bc\bar{s}\bar{s}$	$B_sD_s^*$	$B_s^*D_s$	$S_{bc}A_{ss}$	$B_sD_s^*$	$B_s^*D_s^*$	$A_{bc}S_{ss}$
	$cc\bar{s}\bar{s}$	$D_sD_s^*$	$\cdots$	$A_{cc}A_{ss}$	$D_sD_s^*$	$\cdots$	$\cdots$
$1(1^+)$	$bb\bar{q}\bar{q}$	BB^*	$\cdots$	$A_{bb}A$	BB^*	$\cdots$	$\cdots$
	$bc\bar{q}\bar{q}$	BD^*	B^*D	$S_{bc}A$	BD^*	B^*D^*	$A_{bc}S$
	$cc\bar{q}\bar{q}$	DD^*	$\cdots$	$A_{cc}A$	DD^*	$\cdots$	$\cdots$

components for the meson-meson topologies and the attractive $\bar{\mathbf{3}}\otimes\mathbf{3}$ and repulsive $\mathbf{6}\otimes\bar{\mathbf{6}}$ color tensors for the diquark-antidiquark topology (for details see Supplemental Material in [28]).

It is important to realize that Eq. (4) does not make any assumptions on the internal spatial distribution of the four-quark state. All four topologies, $\mathbf{1}\otimes\mathbf{1}$, $\mathbf{8}\otimes\mathbf{8}$, $\bar{\mathbf{3}}\otimes\mathbf{3}$ and $\mathbf{6}\otimes\bar{\mathbf{6}}$, decode structure in color and flavor space only. It is thus a purely dynamical question related to the details of the interactions between the (anti)quarks which of these topologies dominate, and which internal structure and spatial distribution follows from this dominance.

The procedure we employ to extract the masses of the four-quark states is described in Appendix B of Ref. [30]. We calculate the eigenvalues $\lambda_i(P^2)$ of the four-quark BSE and determine the masses M_i from intersections where the condition $\lambda_i(P^2 = -M_i^2) = 1$ is satisfied. If the states lie above thresholds, we analytically continue the eigenvalues above the thresholds. At present we cannot reliably extract the widths of the resonances, which would require knowledge of the eigenvalues for complex P^2 on the first sheet above the threshold (using contour deformations) and a subsequent analytic continuation to higher Riemann sheets. This procedure has been successfully employed in two-body systems [26,36] but its implementation in the four-body equation remains the subject of future work.

Note that results for spectra of open-flavor four-quark states have already been published by some of us in Ref. [28]. These have been obtained with attractive color forces only and employing an extrapolation method for the eigenvalue curves (second order polynomials) that at the time was considered reliable with errors given in Ref. [28]. In the course of this work, we updated their results using improved extrapolation methods (amongst those higher order polynomials). Corresponding results are presented in Appendix D. While we found that the extrapolation of many states is indeed insensitive to this improvement of methods, the masses of some states do change, e.g., the mass of the T_{cc}^+. We have carefully checked that our improved method is much more robust and are therefore confident to state that the results of this work for open-flavor states supersede those of Ref. [28].

III. RESULTS

A. Spectra and binding energies

Our results for the spectra of open-flavor ground and radially excited $QQ'\bar{q}\bar{q}'$ states with $Q, Q' \in \{b, c\}$, $q = q' \in \{c, s, d, u\}$ and quantum numbers $I(J^P) = 0(1^+)$, $1(1^+)$ are shown in Fig. 2. The corresponding masses are given in Appendix C. We also plot the lowest relevant heavy-light meson-meson thresholds for the respective quantum numbers. The respective meson masses are obtained from the two-body BSE and compiled in Table II in Appendix B.

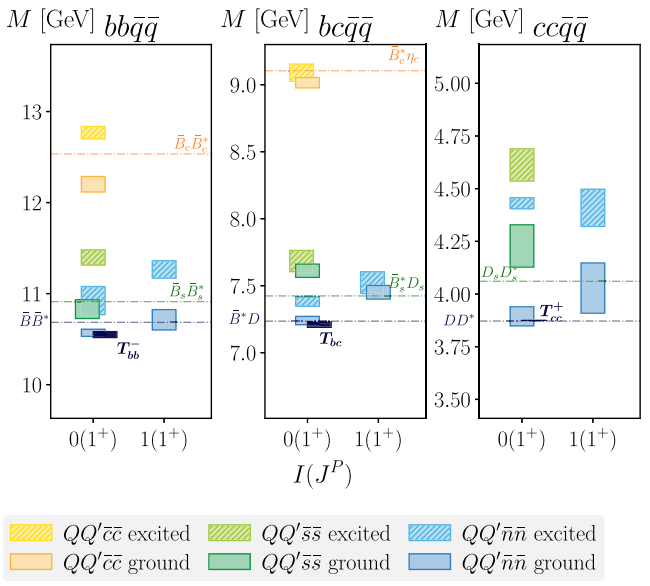

FIG. 2. Spectrum for the open-flavor $J^P = 1^+$ states. From left to right we show the spectra of open-bottom $bb\bar{q}\bar{q}$, open-bottom-charm $bc\bar{q}\bar{q}$ and open-charm $cc\bar{q}\bar{q}$. The heights of the boxes represent the error of the extracted masses. As a reference, we plotted the lowest relevant thresholds (see Table I) for the respective four-quark systems (color coded according to the box color). The black box for the T_{cc}^+ is the only experimentally known state at the time of writing, whereas the boxes for the T_{bb}^- and T_{bc} are the averaged theoretical results.

For the ground states in the $I(J^P) = 0(1^+)$ channel, we find a clear hierarchy for the binding energies, i.e., the $bb\bar{n}\bar{n}$ (with $n \in \{u, d\}$) is deeply bound, the $bc\bar{n}\bar{n}$ is at best shallowly bound, and the $cc\bar{n}\,\bar{n}$ sits right at the DD^* threshold. This matches expectations from the literature: numerous studies including lattice QCD [17,20,21,38–45] identify a potentially deeply bound T_{bb}^- as a $bb\bar{u}\,\bar{d}$ state and predict less binding as the heavy quark mass decreases [38,43,46–52]. This averaged value for the T_{bb}^- from the literature is displayed in the left plot of Fig. 2 in black as a reference. For its binding energy, we find very good agreement with the literature (top left in Fig. 3). The same is true for the T_{bc} (top center in Fig. 3): Our result is slightly above the threshold but still more in accordance with recent lattice results [48,53]. For the experimentally known T_{cc}^+ we find a binding energy of about 20 ± 50 MeV with respect to the DD^* threshold, which is in good agreement with the shallow experimental state with binding energy $\delta m_{\mathrm{BW}} = -273(61)$ keV$/c^2$ [22] (top right in Fig. 3).

The interplay between attractive and repulsive forces is crucial for this agreement. Including only attractive color components yields (much) too strong binding. Depending on quantum numbers, adding the repulsive color components leads to upwards shifts of the masses in the range of 100–400 MeV, see Appendix D for details. Compared to other states, the upwards shift of the T_{cc}^+ mass is quite modest with about 100 MeV.

Regarding the $I(J^P) = 1(1^+)$ states: It is well known, e.g., from lattice QCD [44,45] that the repulsive forces are stronger for $I = 1$ than for $I = 0$ leading to unbound states. Indeed, we also find these states to be unbound (bottom row in Fig. 3).

For ground states with $\bar{s}\,\bar{s}$ quark content we see the same mass hierarchy from $QQ = bb$, $QQ = bc$ to $QQ = cc$ as for the states with light quark content. In the $QQ = bb$ channel, the double-strange ground state is still below threshold, with a difference between double-light and double-strange ground states of about 250 MeV (compared to about 340 MeV for the $QQ = cc$ states).

For the radial excitations, however, we find an interesting different pattern. We have chosen the mass ranges in the spectra of Fig. 2 such that relative excitation energies with respect to the lowest threshold can be directly compared between the three channels. For the radial excitations, the relative excitation energy is clearly smallest in the $QQ = bc$ channel. We currently have no obvious explanation of this behavior but suspect that the different symmetry structure of unequal heavy quarks bc vs equal heavy quarks cc, bb plays an important role.

Finally, we note that our heaviest states ($bb\bar{c}\bar{c}$, $bc\bar{c}\bar{c}$) are strongly bound. Whether this binding is too strong remains to be investigated. Lattice studies in the Born-Oppenheimer approximation seem to exclude bound $bb\bar{c}\bar{c}$ states [44] but one may argue that the Born-Oppenheimer approximation in this case is perhaps not entirely free of doubt.

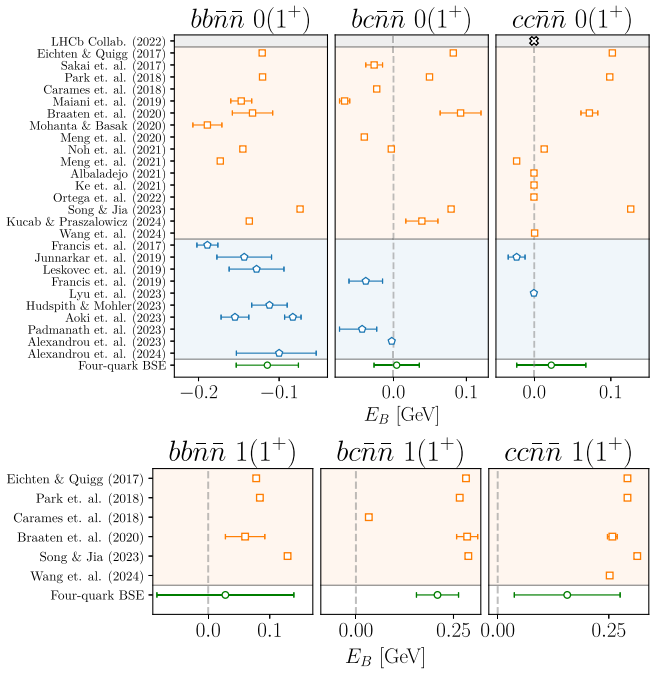

FIG. 3. Comparison of theoretical and (if available) experimental results for the binding energy E_B of the $J^P = 1^+$ ground states. The results in green are from this work. The blue points are lattice results [17,20,21,38–40,46–48,53] and the orange ones from phenomenology [18,19,41,54–66]. The grey dashed lines are the lowest meson-meson thresholds for the respective channel.

B. Internal structure

The main novel element of our study compared to other approaches is the possibility to identify internal structures in terms of clustering of meson and diquark pairs, namely through norm contributions [30]: One takes the physical amplitude in Eq. (4), in this case consisting of six elements, and contracts it with its charge conjugate $\bar{\Gamma}^{(\mu)}$ (connected by quark propagators). This yields 6×6 diagrams, where the diagonal elements are the strengths from each physical component in Table I and the off-diagonal ones describe their mixing (see Appendix E for details). The results are given in Fig. 4.

In general, we find significant and interesting differences between states with different flavor and isospin. In the $I(J^P) = 0(1^+)$ tower, the $cc\bar{n}\bar{n}$ state (the T_{cc}^+) is clearly special as it is almost purely determined by the attractive DD^* contribution. This may be expected since its mass is extremely close to the DD^* threshold and it is thus a prime candidate for a meson molecule. From our current formalism we cannot asses the spatial extent of this state and thus we can neither confirm nor discard the notion that the D and D^* components are far apart. Nevertheless it is striking that the underlying dynamics of dressed one-gluon exchange is capable of dynamically producing such a state. This is even more interesting as other flavor combinations

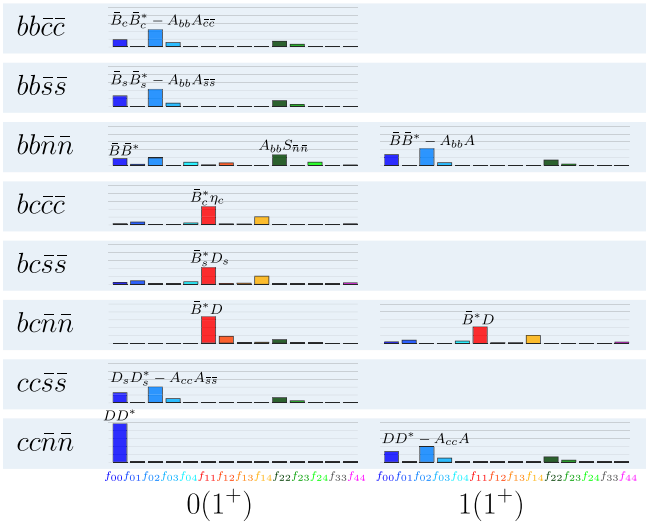

FIG. 4. Norm contributions for the ground states in the axial-vector $J^P = 1^+$ channel with $I = 0, 1$. The results for the excited states (not shown) are very similar. The distance between two horizontal lines in the bar plots is 20%. Note that $I = 1$ states with $\bar{s}\,\bar{s}$ and $\bar{c}\,\bar{c}$ do not exist.

show a completely different picture. The $bb\bar{n}\,\bar{n}$ bottom partner (the T_{bb}^-) is much more diverse. Here we find a dominant attractive diquark $A_{bb}S$ component with about 32% (dark green) contribution, followed by its mixing with the attractive BB^* component (19%, light blue) and the BB^* contribution itself (18%, dark blue). The other components are all below 10%. These findings qualitatively agree with lattice studies [67] (although it may not be entirely clear whether the mixings are directly comparable). The situation changes again for the T_{bc} with $bc\bar{n}\bar{n}$, which is strongly dominated by the attractive $\bar{B}^*D$ component (70%, red), whose mixing with the attractive $A_{bc}S$ component (18%, orange red) is also quite prominent. This pattern is different from both bb and cc and can be attributed to the different symmetries in the bc case [68,69], which we confirm dynamically from the underlying QCD interaction.

It is also striking to see the effect of changed symmetries in the different isospin channels: Whereas in the $I(J^P) = 0(1^+)$ tower we find significant differences between T_{cc}^+ and T_{bb}^-, such differences are absent for $I(J^P) = 1(1^+)$. Both $QQ\bar{n}\bar{n}$ states in this case are dominated by the mixing effects of the meson-meson component with the attractive diquark components.

IV. CONCLUSIONS

In this work we studied the masses and binding energies of open-flavor four-quark states with two heavy quarks, $Q, Q' \in \{b, c\}$, using functional methods in QCD, employing Dyson-Schwinger equations and a four-body Faddeev-Yakubowski equation. Assuming dominance of two-body correlations, we demonstrated that the interactions between the four quarks can create very different internal structures depending on the flavor content. The T_{cc}^+ is completely dominated by DD^* components due to its proximity to the respective threshold, whereas the T_{bb}^- is deeply bound and its internal structure is a complicated mixture of meson-meson and diquark components. The pattern with variations of flavor and isospin, discussed around Fig. 4, emerges from the same underlying interaction, namely dressed gluon exchange in rainbow-ladder approximation, which dynamically creates meson and diquark clusters without further assumptions. The quantitative results for the binding energies are highly nontrivial and very encouraging results in our approach. Similar analyses for hidden-flavor and other open-flavor states are subject to future work as well as further systematic studies regarding the quality of our approximations.

ACKNOWLEDGMENTS

We thank Marc Wagner and the Frankfurt group for pointing out the importance of the repulsive color channels and for extended and very fruitful discussions on the subject. This work was supported by the BMBF under Project No. 05P2021, the DFG under Grant No. FI 970/11-2, the graduate school HGS-HIRe and the GSI Helmholtzzentrum für Schwerionenforschung. This work contributes to the aims of the U.S. Department of Energy ExoHad Topical Collaboration, Contract No. DE-SC0023598. We acknowledge computational resources provided by the HPC Core Facility and the HRZ of the Justus-Liebig-Universität Gießen.

APPENDIX A: CONSTRUCTION OF OPEN-FLAVOR AMPLITUDES FOR UNEQUAL QUARKS

Open-flavor four-quark states with quark content $QQ'\bar{q}\bar{q}'$ do not obey charge-conjugation symmetry, but rather the wave function of the state is subject to Pauli antisymmetry under the exchange of $Q \leftrightarrow Q'$ or $\bar{q} \leftrightarrow \bar{q}'$. The tensor bases for the quantum numbers investigated in this work were constructed accordingly and can be found in the Supplemental Material of [28]. However, these works only considered open-flavor states with equal heavy-quark pairs QQ'. For an unequal heavy-quark pair bc, the Pauli antisymmetry does not hold when exchanging b and c quarks. Therefore, these bases need to be modified to investigate these states.

Given the necessary Dirac-color tensors to construct an axial-vector tetraquark with $J^P = 1^+$, i.e., Eq. (A10) in the Supplemental Material of [28], one can arrange these tensors in four "categories," denoted by $\Psi_{(s/a)(s/a)}$. Each fulfils a certain Pauli symmetry (s) or antisymmetry (a) when exchanging $Q \leftrightarrow Q'$ or $\bar{q} \leftrightarrow \bar{q}'$ depending on the flavor wave function. These are (i) both Pauli symmetric (Ψ_{ss}), (ii) both Pauli antisymmetric (Ψ_{aa}), (iii) symmetric under $Q \leftrightarrow Q'$ and antisymmetric under $\bar{q} \leftrightarrow \bar{q}'$ (Ψ_{sa}), and

(iv) antisymmetric under $Q \leftrightarrow Q'$ and symmetric under $\bar{q} \leftrightarrow \bar{q}'$ (Ψ_{as}). To make a state with equal heavy-quark pair and $I(J^P) = 0(1^+)$, one needs the tensors to be antisymmetric when exchanging the heavy-quark pair and symmetric when exchanging the light, i.e., Ψ_{as}. This then yields the components DD^*, D^*D^* and $A_{cc}S$ for the $cc\bar{q}\bar{q}$ and BB^*, B^*B^* and $A_{bb}S$ for the $bb\bar{q}\bar{q}$ state. However, for an unequal heavy-quark pair there is no symmetry when exchanging $Q \leftrightarrow Q'$, whereas the symmetry in $\bar{q} \leftrightarrow \bar{q}'$ is still present. One can then form a linear combination of the tensors in Ψ_{as} with the tensors in Ψ_{ss}, effectively destroying the (anti)symmetry in the first index of Ψ while retaining the symmetry in the second index, i.e., $\bar{q} \leftrightarrow \bar{q}'$. This disentangles the basis elements for the pseudoscalar-vector heavy-light meson-meson components, which then yields the following components for the $0(1^+)$ with quark content $bc\bar{q}\bar{q}'$: $\bar{B}D^*$, $\bar{B}^*D$, $\bar{B}^*D^*$ and $A_{bc}S$. We neglect the attractive $\bar{B}^*D^*$ in the physical components in Table I as it is the highest of the heavy-light meson-meson thresholds and was found to have negligible effect on the mass. However, for the isospin $I = 1$ $bc\bar{q}\bar{q}$ states, the repulsive $\bar{B}^*D^*$ component was found to significantly contribute to the mass, pushing it into the correct region.

A further note has to be made regarding the color basis elements. The respective combinations that make up an overall color singlet are given in the Supplemental Material of [28]. From $\mathbf{3} \otimes \mathbf{3} \otimes \bar{\mathbf{3}} \otimes \bar{\mathbf{3}} = (\bar{\mathbf{3}} \oplus \mathbf{6}) \otimes (\mathbf{3} \oplus \bar{\mathbf{6}}) = \mathbf{1} \oplus \mathbf{1} \oplus \ldots$, the color part of the amplitude consists of two independent color singlet tensors. These include the attractive meson-meson color wave functions

$$C_{11} = \frac{1}{3}\delta_{AC}\delta_{BD}, \qquad C'_{11} = \frac{1}{3}\delta_{AD}\delta_{BC},$$

the attractive and repulsive diquark-antidiquark color wave functions

$$C_{\bar{3}3} = -\frac{\sqrt{3}}{2}(C_{11} - C'_{11}), \quad C_{6\bar{6}} = \sqrt{\frac{3}{8}}(C_{11} + C'_{11}),$$

and the repulsive meson-meson

$$C_{88} = \frac{C_{11} - 3C'_{11}}{2\sqrt{2}}, \quad C'_{88} = \frac{C'_{11} - 3C_{11}}{2\sqrt{2}}$$

components, where $A, B, C, D = 1, 2, 3$ denote the color indices. Under Pauli symmetry, these tensors transform as follows:

$$C_{11} \leftrightarrow C'_{11}, \quad C_{88} \leftrightarrow C'_{88}, \tag{A1}$$

$$C_{\bar{3}3} \leftrightarrow -C_{\bar{3}3}, \quad C_{6\bar{6}} \leftrightarrow C_{6\bar{6}}. \tag{A2}$$

While the meson-meson component stays the same[2] in Table I for the attractive and repulsive channels due to Eq. (A1), the different sign in the symmetry transformations of Eq. (A2) forces the repulsive diquark-antidiquark Dirac-color tensors to fulfil the "mirrored" Pauli symmetry from the attractive diquark-antidiquark tensors, e.g., Ψ_{as} for attractive $\rightarrow \Psi_{sa}$ for the repulsive channel. Therefore, different diquark-antidiquark components appear in f_2 and f_5 in Table I.

[2]For the $1(1^+)$ $bc\bar{q}\bar{q}$ and $0(1^+)$ $bc\bar{s}\bar{s}$ states the repulsive $\bar{B}^*D^*$ component was found to be more significant than the repulsive $\bar{B}^*D$ component.

APPENDIX B: TWO-BODY INTERACTION

We employ a rainbow-ladder truncation combined with the effective Maris-Tandy (MT) interaction [70,71] for the two-body interaction kernels, which has proven to be a very successful approximation in the functional framework. For recent reviews on the application to the meson, baryon and four-quark phenomenology in the past, see [34,35]. This interaction has also been used to compute the quark Dyson-Schwinger equation and the meson and diquark mass spectrum obtained from the quark-(anti)quark BSE (see Table II), both of which are needed as input for the four-quark BSE. The interaction in its explicit form can be found in Eq. (3.96) of [34]; in this work we use the scale parameter $\Lambda = 0.72$ tuned to reproduce the pion decay constant and fix the shape parameter to $\eta^{\mathrm{MT}} = 1.8$. The MT interaction describes the phenomenology of light mesons in the pseudoscalar and vector channel reasonably well, whereas the results in the scalar and axial-vector channels are not satisfactory. The qualitative reliability of the interaction can be judged from the two-body meson masses

TABLE II. $Q\bar{q}$ mesons with quantum numbers $J^{PC} = \{0^{-+}, 1^{--}\}$ grouped according to their quark model classification. We show the experimental candidates [37], the masses m_{RL} obtained in our rainbow-ladder calculation, and the relative error of these to the masses given in the particle data group (PDG) (if the experimental state has been identified). In the last two columns we also show the obtained rainbow-ladder masses for the corresponding Qq diquarks with quantum numbers $J^P = \{0^+, 1^+\}$. All values are given in MeV.

	0^{-+}			1^{--}			0^+	1^+
	PDG	m_{RL}	$\Delta m^{\mathrm{rel.}}$	PDG	m_{RL}	$\Delta m^{\mathrm{rel.}}$	m_{0^+}	m_{1^+}
$n\bar{n}$	π/η[a]	137	0.0%	ρ/ω	736	5.2%	809	1006
$s\bar{n}$	K	501	1.1%	K^*	913	0.1%	1072	1259
$s\bar{s}$	$\cdots$	698	$\cdots$	ϕ	1070	5.0%	1266	1412
$c\bar{n}$	D	1860	0.4%	D^*	2011	0.1%	2421	2439
$c\bar{s}$	D_s	1937	1.6%	D_s^*	2124	0.5%	2523	2543
$c\bar{c}$	η_c	2803	6.1%	J/ψ	2992	3.4%	3415	3433
$b\bar{n}$	B	5310	0.6%	B^*	5375	0.9%	6396	6403
$b\bar{s}$	B_s	5425	1.1%	B_s^*	5487	1.3%	6473	6492
$b\bar{c}$	B_c	6232	0.7%	$\cdots$	6302	$\cdots$	7139	7269
$b\bar{b}$	η_b	9421	0.2%	Υ	9500	0.4%	9915	10394

[a]The π and the η are mass degenerate in this work, since we neglect the strange component in the η and the indirect effect of the topological mass via octet-singlet mixing.

displayed in Table I in Ref. [30]. Herein, for the convenience of the reader, we display in Table II again the masses of the pseudoscalar and vector mesons that enter our calculation.

At the quark level, and consequently also at the meson level, we work in the isospin symmetric limit, i.e., $m_{\pi^\pm} = m_{\pi^0}$, $m_{D^\pm} = m_{D^0}$, $m_{B^\pm} = m_{B^0}$. The u/d current-quark mass is fixed by m_π. The strange, charm and bottom quark masses are fixed such that the following criteria are satisfied: the sums $m_D + m_{D^*}$, $m_{D_s} + m_{D_s^*}$ and $m_B + m_{B^*}$ have to match the sum of the respective experimental values [37] within 1% relative error. Note, however, that the isospin limit is broken at the level of the four-point functions by symmetries and the potential appearance of attractive and repulsive channels displayed in Table I.

APPENDIX C: MASSES AND BINDING ENERGIES OF OPEN FLAVOUR FOUR-QUARK STATES

In Tables III and IV we give explicit numbers for the masses and binding energies of the states discussed in the main body of this work in Sec. III.

TABLE III. Ground-state masses (upper panel) and first radial excitations (lower panel) for the open-charm ($cc\bar{q}\bar{q}$) and open-bottom ($bb\bar{q}\bar{q}$) states in GeV. For completeness we also display the binding energies E_B with respect to the lightest (calculated) heavy-light meson-meson threshold in each channel; the "binding energies" for resonant particles above the threshold are shown in bold. The error given in the brackets is the combination of the extrapolation error and the error of the fit to the quark mass evolution curve.

	$0(1^+)$		$1(1^+)$	
	M	E_B	M	E_B
$cc\bar{n}\bar{n}$	3.89(5)	**0.02(5)**	4.03(12)	**0.16(12)**
$cc\bar{s}\bar{s}$	4.23(10)	**0.17(10)**	…	…
$bb\bar{n}\bar{n}$	10.57(4)	−0.11(4)	10.71(11)	**0.03(11)**
$bb\bar{s}\bar{s}$	10.83(10)	−0.08(10)	…	…
$bb\bar{c}\bar{c}$	12.20(9)	−0.33(9)	…	…

	$0(1^+)$		$1(1^+)$	
	M	E_B	M	E_B
$cc\bar{n}\bar{n}$	4.43(3)	**0.56(3)**	4.41(9)	**0.54(9)**
$cc\bar{s}\bar{s}$	4.61(8)	**0.55(8)**	…	…
$bb\bar{n}\bar{n}$	10.92(15)	**0.24(15)**	11.27(10)	**0.58(10)**
$bb\bar{s}\bar{s}$	11.40(8)	**0.49(8)**	…	…
$bb\bar{c}\bar{c}$	12.77(7)	**0.23(7)**	…	…

TABLE IV. Ground-state and excited state masses in GeV for four-quark states $QQ'\bar{q}\bar{q}'$ with unequal heavy QQ' pair. We also display the binding energies with respect to the lowest relevant meson-meson thresholds, i.e., B^*D for the 1^+ state. Masses of resonant particles are above the thresholds and their "binding energies" are shown in bold.

	$0(1^+)$		$1(1^+)$	
	M	E_B	M	E_B
$bc\bar{n}\bar{n}$	7.24(3)	**0.00(3)**	7.45(5)	**0.22(5)**
$bc\bar{s}\bar{s}$	7.61(5)	**0.19(5)**	…	…
$bc\bar{c}\bar{c}$	9.02(1)	−0.09(1)	…	…
$bc\bar{b}\bar{b}$	14.86(1)	−0.88(1)	…	…

	$0(1^+)$		$1(1^+)$	
	M	E_B	M	E_B
$bc\bar{n}\bar{n}$	7.38(3)	**0.15(3)**	7.52(8)	**0.29(8)**
$bc\bar{s}\bar{s}$	7.68(8)	**0.26(8)**	…	…
$bc\bar{c}\bar{c}$	9.09(6)	−0.01(6)	…	…
$bc\bar{b}\bar{b}$	14.94(0)	−0.79(0)	…	…

APPENDIX D: OPEN-FLAVOR SPECTRUM WITH ONLY ATTRACTIVE COLOR FORCES

In Fig. 5 we show the spectrum for the $J^P = 1^+$ states where we only took the attractive color components in Table I into account. The corresponding numerical values are given in Tables V and VI. We can now compare this spectrum to the one in Fig. 2, where the attractive and repulsive color components were used.

Starting with the open-bottom spectrum, we find that the mass of the $bb\bar{n}\bar{n}$ ground state in the $0(1^+)$ channel moves up by about 400 MeV when we include the repulsive color channels. The mass of the corresponding excited state in

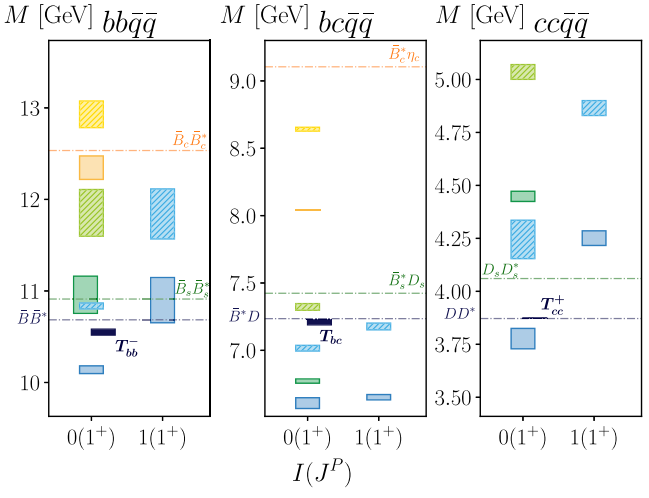

FIG. 5. Same plot as in Fig. 2, but here we show the spectra obtained by only including the attractive components given in Table I.

TABLE V. Masses and binding energies with respect to the lowest meson-meson threshold for the ground-state (upper panel) and first radial excitations (lower panel) for the open-charm ($cc\bar{q}\,\bar{q}$) and open-bottom ($bb\bar{q}\,\bar{q}$) states obtained by using the attractive color components only. The corresponding spectrum is shown in Fig. 5. Masses are given in GeV.

	$0(1^+)$		$1(1^+)$	
	M	E_B	M	E_B
$cc\bar{n}\bar{n}$	3.78(5)	−0.09(5)	4.25(3)	**0.38**(**3**)
$cc\bar{s}\bar{s}$	4.45(2)	**0.39**(**2**)	⋯	⋯
$bb\bar{n}\bar{n}$	10.14(4)	−0.54(4)	10.90(25)	**0.21**(**25**)
$bb\bar{s}\bar{s}$	10.96(20)	**0.05**(**20**)	⋯	⋯
$bb\bar{c}\bar{c}$	12.35(13)	−0.19(13)	⋯	⋯

	$0(1^+)$		$1(1^+)$	
	M	E_B	M	E_B
$cc\bar{n}\bar{n}$	4.25(9)	**0.37**(**9**)	4.87(4)	**0.99**(**4**)
$cc\bar{s}\bar{s}$	5.04(3)	**0.97**(**3**)	⋯	⋯
$bb\bar{n}\bar{n}$	10.84(3)	**0.15**(**3**)	11.84(27)	**1.16**(**27**)
$bb\bar{s}\bar{s}$	11.85(25)	**0.94**(**25**)	⋯	⋯
$bb\bar{c}\bar{c}$	12.93(15)	**0.40**(**15**)	⋯	⋯

TABLE VI. Ground-state and excited state masses in GeV for four-quark states $QQ'\bar{q}\bar{q}'$ with unequal heavy QQ' pair when only using the attractive color channels. We also display the binding energies with respect to the lowest relevant meson-meson thresholds, i.e., B^*D for the 1^+ state. Masses of resonant particles are above the thresholds and their "binding energies" are shown in bold.

	$0(1^+)$		$1(1^+)$	
	M	E_B	M	E_B
$bc\bar{n}\bar{n}$	6.61(4)	−0.63(4)	6.65(2)	−0.58(2)
$bc\bar{s}\bar{s}$	6.77(2)	−0.65(2)	⋯	⋯
$bc\bar{c}\bar{c}$	8.04(0)	−1.07(0)	⋯	⋯
$bc\bar{b}\bar{b}$	14.01(1)	−1.72(1)	⋯	⋯

	$0(1^+)$		$1(1^+)$	
	M	E_B	M	E_B
$bc\bar{n}\bar{n}$	7.02(2)	−0.22(2)	7.18(2)	−0.06(2)
$bc\bar{s}\bar{s}$	7.32(2)	−0.10(2)	⋯	⋯
$bc\bar{c}\bar{c}$	8.64(1)	−0.46(1)	⋯	⋯
$bc\bar{b}\bar{b}$	14.53(1)	−1.20(1)	⋯	⋯

this channel increases by about 800 MeV with the caveat that the error bar here is quite large. By including the repulsive color forces, the masses of the ground and excited states with $bb\bar{q}\bar{q}$ and $\bar{q} \neq \bar{n}$ can be determined more accurately compared to the attractive color channels only case, leading to a reduction in error (cf. upper panels of Table III and Table V). Same goes for the $bb\bar{n}\bar{n}$ ground and excited state with $1(1^+)$.

For the $bc\bar{q}\bar{q}$ states one can see that without the inclusion of the repulsive color channels, the whole spectrum is found to be very deeply bound. Thus, the consideration of attractive and repulsive color forces is of vital importance here, as the whole spectrum gets shifted upwards by 300 to 900 MeV into the correct mass region.

Regarding the open-charm spectrum, the $cc\bar{n}\bar{n}$ ground state in the $0(1^+)$ channel increases in mass by about 120 MeV when including the repulsive color channels. This moves the state right up to the DD^* threshold, where it is expected from experiment [37].

As explained in the main part of this work, the results displayed in Fig. 5 have been obtained with improved extrapolation methods as compared to the previous work by some of us, Ref. [28]. Thus they supersede those of Ref. [28] as concerns the open-flavor states.

APPENDIX E: NORM CONTRIBUTION QUARK MASS EVOLUTION CURVES

To calculate the norm contributions in Fig. 4, the four-quark states must be on shell. However, because the on-shell BSE is not always directly calculable due to internal two-body poles, we vary the mass of the "light" $\bar{q}\bar{q}$ pair from $\bar{n}\,\bar{n}$ to $\bar{b}\,\bar{b}$ to determine the quark mass evolution of the norm contributions. Their extrapolation to the physical u/d quark mass then yields the result in Fig. 4.

Figure 6 shows the quark mass evolution of the norm contributions in the $0(1^+)$ (top row) and $1(1^+)$ (bottom row) channels for the $cc\bar{q}\bar{q}$ (left column) and $bb\bar{q}\bar{q}$ states (right column). The analogous case for $bc\bar{q}\bar{q}$ with $0(1^+)$ is shown in Fig. 7. The different data points represent the correlations between the internal clusters given in Table I, and the corresponding fits are colored accordingly. To obtain each data point, we calculate the norm contribution at each P^2 in the eigenvalue curve and read off the result where the condition $\lambda(P^2) = 1$ is satisfied. For most states, the curves do not show much changes over the whole mass range from up/down to the bottom quark region. This is exceptionally different for the T_{cc}^+, which shows dominance of the DD^* for "light" quark pairs only below about the charm quark mass $m_q < m_c$.

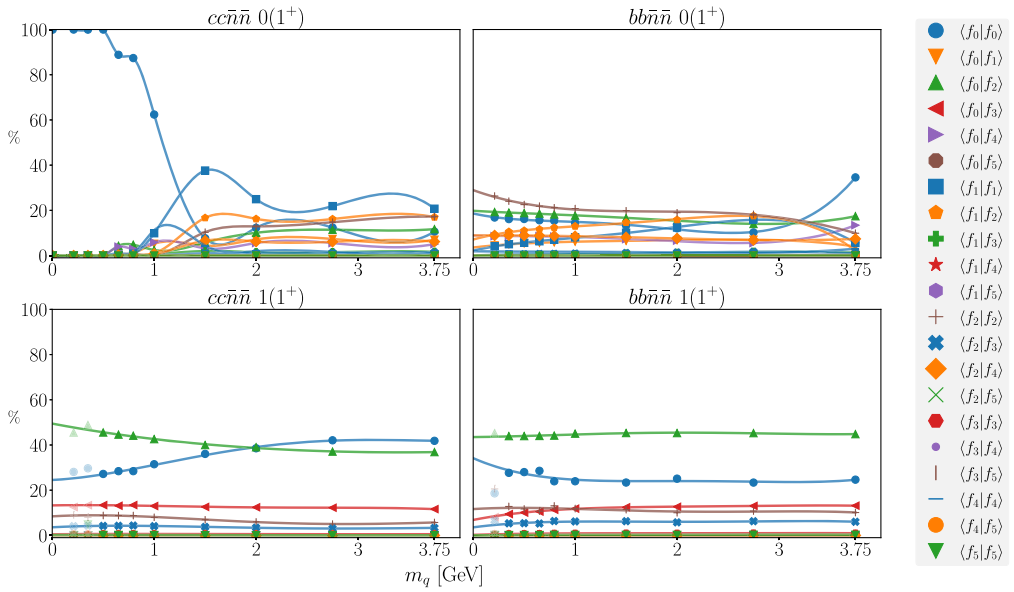

FIG. 6. Quark mass evolution of the norm contributions for the equal heavy-quark pair ground states in the $0(1^+)$ (top row) and the $1(1^+)$ (bottom row) channel. The left panels show the charm ($cc\bar{q}\bar{q}$) and the right panels the bottom ($bb\bar{q}\bar{q}$) states. The colors of the fits correspond to the fitted data points. Data points depicted as opaque were not taken into account in the fits.

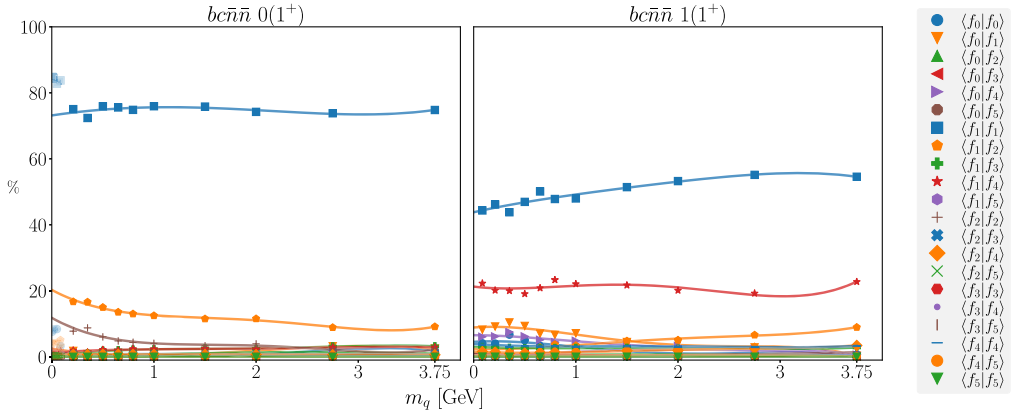

FIG. 7. Norm contribution quark mass evolution curves for the unequal heavy-quark pair ground states in the $0(1^+)$ and $1(1^+)$ channels. The colors of the fits correspond to the fitted data points. Data points depicted as opaque were not taken into account in the fits.

[1] M. Gell-Mann, Phys. Lett. **8**, 214 (1964).
[2] S.-K. Choi *et al.* (Belle Collaboration), Phys. Rev. Lett. **91**, 262001 (2003).
[3] H.-X. Chen, W. Chen, X. Liu, and S.-L. Zhu, Phys. Rep. **639**, 1 (2016).
[4] A. Esposito, A. Pilloni, and A. Polosa, Phys. Rep. **668**, 1 (2017).
[5] R. F. Lebed, R. E. Mitchell, and E. S. Swanson, Prog. Part. Nucl. Phys. **93**, 143 (2017).
[6] A. Ali, J. S. Lange, and S. Stone, Prog. Part. Nucl. Phys. **97**, 123 (2017).
[7] F.-K. Guo, C. Hanhart, U.-G. Meißner, Q. Wang, Q. Zhao, and B.-S. Zou, Rev. Mod. Phys. **90**, 015004 (2018).
[8] S. L. Olsen, T. Skwarnicki, and D. Zieminska, Rev. Mod. Phys. **90**, 015003 (2018).
[9] Y.-R. Liu, H.-X. Chen, W. Chen, X. Liu, and S.-L. Zhu, Prog. Part. Nucl. Phys. **107**, 237 (2019).

[10] N. Brambilla, S. Eidelman, C. Hanhart, A. Nefediev, C.-P. Shen, C. E. Thomas, A. Vairo, and C.-Z. Yuan, Phys. Rep. **873**, 1 (2020).
[11] S. Navas *et al.* (Particle Data Group), Phys. Rev. D **110**, 030001 (2024).
[12] J. Ballot and J. Richard, Phys. Lett. **123B**, 449 (1983).
[13] S. Zouzou, B. Silvestre-Brac, C. Gignoux, and J. M. Richard, Z. Phys. C Part. Fields **30**, 457 (1986).
[14] H. J. Lipkin, Phys. Lett. B **172**, 242 (1986).
[15] L. Heller and J. A. Tjon, Phys. Rev. D **35**, 969 (1987).
[16] A. V. Manohar and M. B. Wise, Nucl. Phys. **B399**, 17 (1993).
[17] A. Francis, R. Hudspith, R. Lewis, and K. Maltman, Phys. Rev. Lett. **118**, 142001 (2017).
[18] E. J. Eichten and C. Quigg, Phys. Rev. Lett. **119**, 202002 (2017).
[19] E. Braaten, L.-P. He, and A. Mohapatra, Phys. Rev. D **103**, 016001 (2021).
[20] R. Hudspith and D. Mohler, Phys. Rev. D **107**, 114510 (2023).
[21] C. Alexandrou, J. Finkenrath, T. Leontiou, S. Meinel, M. Pflaumer, and M. Wagner, Phys. Rev. D **110**, 054510 (2024).
[22] R. Aaij *et al.* (LHCb Collaboration), Nat. Commun. **13**, 3351 (2022).
[23] R. Aaij *et al.* (LHCb Collaboration), Nat. Phys. **18**, 751 (2022).
[24] W. Heupel, G. Eichmann, and C. S. Fischer, Phys. Lett. B **718**, 545 (2012).
[25] G. Eichmann, C. S. Fischer, and W. Heupel, Phys. Lett. B **753**, 282 (2016).
[26] N. Santowsky and C. S. Fischer, Phys. Rev. D **105**, 034025 (2022).
[27] P. C. Wallbott, G. Eichmann, and C. S. Fischer, Phys. Rev. D **100**, 014033 (2019).
[28] P. C. Wallbott, G. Eichmann, and C. S. Fischer, Phys. Rev. D **102**, 051501 (2020).
[29] N. Santowsky and C. S. Fischer, Eur. Phys. J. C **82**, 313 (2022).
[30] J. Hoffer, G. Eichmann, and C. S. Fischer, Phys. Rev. D **109**, 074025 (2024).
[31] G. Eichmann, C. S. Fischer, and W. Heupel, Phys. Rev. D **92**, 056006 (2015).
[32] K. Huang and H. A. Weldon, Phys. Rev. D **11**, 257 (1975).
[33] A. N. Kvinikhidze and A. M. Khvedelidze, Theor. Math. Phys. **90**, 62 (1992).
[34] G. Eichmann, H. Sanchis-Alepuz, R. Williams, R. Alkofer, and C. S. Fischer, Prog. Part. Nucl. Phys. **91**, 1 (2016).
[35] G. Eichmann, C. S. Fischer, W. Heupel, and N. Santowsky, and P. C. Wallbott, Few-Body Syst. **61**, 38 (2020).
[36] G. Eichmann, P. Duarte, M. Peña, and A. Stadler, Phys. Rev. D **100**, 094001 (2019).
[37] R. L. Workman *et al.* (Particle Data Group), Prog. Theor. Exp. Phys. **2022**, 083C01 (2022).
[38] P. Junnarkar, N. Mathur, and M. Padmanath, Phys. Rev. D **99**, 034507 (2019).
[39] L. Leskovec, S. Meinel, M. Pflaumer, and M. Wagner, Phys. Rev. D **100**, 014503 (2019).
[40] T. Aoki, S. Aoki, and T. Inoue, Phys. Rev. D **108**, 054502 (2023).
[41] P. Mohanta and S. Basak, Phys. Rev. D **102**, 094516 (2020).
[42] P. Bicudo and M. Wagner (European Twisted Mass Collaboration), Phys. Rev. D **87**, 114511 (2013).
[43] R. Hudspith, B. Colquhoun, A. Francis, R. Lewis, and K. Maltman, Phys. Rev. D **102**, 114506 (2020).
[44] P. Bicudo, K. Cichy, A. Peters, B. Wagenbach, and M. Wagner, Phys. Rev. D **92**, 014507 (2015).
[45] P. Bicudo, K. Cichy, A. Peters, and M. Wagner, Phys. Rev. D **93**, 034501 (2016).
[46] A. Francis, R. J. Hudspith, R. Lewis, and K. Maltman, Phys. Rev. D **99**, 054505 (2019).
[47] Y. Lyu, S. Aoki, T. Doi, T. Hatsuda, Y. Ikeda, and J. Meng, Phys. Rev. Lett. **131**, 161901 (2023).
[48] C. Alexandrou, J. Finkenrath, T. Leontiou, S. Meinel, M. Pflaumer, and M. Wagner, Phys. Rev. Lett. **132**, 151902 (2024).
[49] S. Meinel, M. Pflaumer, and M. Wagner, Phys. Rev. D **106**, 034507 (2022).
[50] A. Radhakrishnan, M. Padmanath, and N. Mathur, Phys. Rev. D **110**, 034506 (2024).
[51] M. Padmanath and S. Prelovsek, Phys. Rev. Lett. **129**, 032002 (2022).
[52] G. K. C. Cheung, C. E. Thomas, J. J. Dudek, and R. G. Edwards (Hadron Spectrum Collaboration), J. High Energy Phys. 11 (2017) 033.
[53] M. Padmanath, A. Radhakrishnan, and N. Mathur, Phys. Rev. Lett. **132**, 201902 (2024).
[54] S. Sakai, L. Roca, and E. Oset, Phys. Rev. D **96**, 054023 (2017).
[55] W. Park, S. Noh, and S. Lee, Acta Phys. Pol. B **50**, 1151 (2019).
[56] T. Caramés, J. Vijande, and A. Valcarce, Phys. Rev. D **99**, 014006 (2019).
[57] L. Maiani, A. D. Polosa, and V. Riquer, Phys. Rev. D **100**, 074002 (2019).
[58] Q. Meng, E. Hiyama, A. Hosaka, M. Oka, P. Gubler, K. Can, T. Takahashi, and H. Zong, Phys. Lett. B **814**, 136095 (2021).
[59] S. Noh, W. Park, and S. H. Lee, Phys. Rev. D **103**, 114009 (2021).
[60] Q. Meng, M. Harada, E. Hiyama, A. Hosaka, and M. Oka, Phys. Lett. B **824**, 136800 (2022).
[61] M. Albaladejo, Phys. Lett. B **829**, 137052 (2022).
[62] H.-W. Ke, X.-H. Liu, and X.-Q. Li, Eur. Phys. J. C **82**, 144 (2022).
[63] P. Ortega, J. Segovia, D. Entem, and F. Fernández, Phys. Lett. B **841**, 137918 (2023).
[64] Y.-X. Song and D.-J. Jia, Commun. Theor. Phys. **75**, 055201 (2023).
[65] D. Wang, K.-R. Song, W.-L. Wang, and F. Huang, Phys. Rev. D **109**, 074026 (2024).
[66] M. Kucab and M. Praszalowicz, Phys. Rev. D **109**, 076005 (2024).
[67] P. Bicudo, A. Peters, S. Velten, and M. Wagner, Phys. Rev. D **103**, 114506 (2021).
[68] H. Garcilazo and A. Valcarce, Few-Body Syst. **61**, 24 (2020).
[69] C. Deng and S.-L. Zhu, Phys. Rev. D **105**, 054015 (2022).
[70] P. Maris and C. D. Roberts, Phys. Rev. C **56**, 3369 (1997).
[71] P. Maris and P. C. Tandy, Phys. Rev. C **60**, 055214 (1999).